Materials Characterization of Alternative Gate Dielectrics

Brett W. Busch, Olivier Pluchery, Yves J. Chabal, David A. Muller, Robert L. Opila, J. Raynien Kwo, and Eric Garfunkel

Abstract

Continued scaling of microelectronic devices is demanding that alternatives to SiO_2 as the gate dielectric be developed soon. This in turn has placed enormous pressure on the abilities of physical characterization techniques to address critical issues such as film and interface structure and composition, transport properties, and thermal or chemical stability. This article summarizes the strengths and capabilities of four techniques used for the materials characterization of alternative gate dielectrics: scanning transmission electron microscopy (STEM) in conjunction with electron energy-loss spectroscopy (EELS), medium-energy ion scattering (MEIS), infrared-absorption spectroscopy (IRAS), and x-ray photoelectron spectroscopy (XPS). The complementary nature of these techniques has allowed for a detailed picture of the various properties of alternative gate dielectrics, and in particular of the dielectric/silicon interface. Critical issues and features of several important alternative gate dielectrics, ZrO_2, Al_2O_3, Y_2O_3, and Gd_2O_3, are explored in light of the well-studied SiO_2/Si system.

Keywords: *chemical structure, electron energy-loss spectroscopy (EELS), high-dielectric-constant materials, high-κ dielectrics, medium-energy ion scattering (MEIS), infrared-absorption spectroscopy (IRAS), physical characterization, scanning transmission electron microscopy (STEM), thin films, x-ray photoelectron spectroscopy (XPS).*

Introduction

One of the more difficult aspects of engineering a viable, alternative high-κ gate dielectric stack has been to determine the structure and composition of a given film. This is especially relevant at the interface, where in order to maintain the advantage of a high-κ material, namely, achieving low electrical thickness (or higher gate capacitance) with a larger physical thickness, one must prevent the formation of a low-κ SiO_x layer during or after film deposition. To this end, physical characterization techniques are necessary in which the composition of a dielectric layer can be determined with a resolution approaching the angstrom level, or alternatively, with a sensitivity better than one monolayer.

In this article, we discuss several powerful experimental methods that we have used to examine high-κ films, focusing on the nature and accuracy of information that they yield. Because of the complexity of the problem, the complementary information that these tools provide is necessary if we are to build up a full atomic-scale understanding of high-κ gate stacks, including their ultimate electrical properties. A key goal of our physical and chemical characterization has been to determine the composition and structure as a function of depth and processing history, with a special emphasis on interface behavior and SiO_2 composition. We first briefly outline key features of each technique, citing some results from the SiO_2/Si system. We then describe a few exemplary results from high-κ systems.

Scanning transmission electron microscopy (STEM) offers a probe as small as 2 Å for imaging buried interfaces viewed in projection. Atomic-resolution images of the lattice provide a calibration of the thickness of the gate stack and interfacial layers. One can also perform electron energy-loss spectroscopy (EELS) using the STEM beam to supply a focused source of incident monochromatic electrons. With this method, one measures the local composition and electronic structure at the atomic scale.[1–3] Each element has a unique EELS binding energy, and a single column of atoms can be excited in favorable cases. The shape of the EELS edge reflects the unoccupied density of states after the core excitation.[4,5]

Atomic-scale EELS has been performed at and near the SiO_2/Si interface.[3,6] Figure 1a shows the EELS oxygen K-edge spectrum obtained at two different points indicated in the annular dark-field (ADF) image of Figure 1b. The interface shows one layer of a sub-stoichiometric oxide whose physical width is ~1.6 Å (Figure 1c).[6] The O K-edge from the interfacial region shows a 3-eV shift down in band edge. EELS measures the electronic width of the interface at 3.5 Å (full width at half maximum, FWHM, of the interfacial region).[6,7] This region should display different dielectric behavior from bulk SiO_2. To first order, the effective interfacial dielectric constant should be ~7–8, halfway between that of Si (κ = 12) and SiO_2 (κ = 3.9). Provided that the SiO_2 layer is kept this thin, the two interfacial layers should not severely reduce the capacitance of the dielectric.

Medium-energy ion scattering (MEIS), in essence a high-resolution variant of standard Rutherford backscattering spectroscopy, is useful for examining films whose thickness is ~1–15 nm.[8] MEIS offers a direct determination of the areal density of elements in a film and, with some understanding of the density and ion-transport behavior, an accurate elemental depth profile. Some additional strengths of MEIS are that it allows simple preparation of samples, it is nondestructive, and it is mass-sensitive, allowing for isotopic studies. MEIS has been successfully used to examine ultrathin silicon oxide and oxynitride films, including showing where and how oxygen and nitrogen incorporate into a growing film.[9,10] Using isotope methods, MEIS was the key tool that allowed one to quantify under what conditions and thickness the classical Deal–Grove oxidation model (involving diffusion of oxygen through the SiO_2 film, where it reacts with

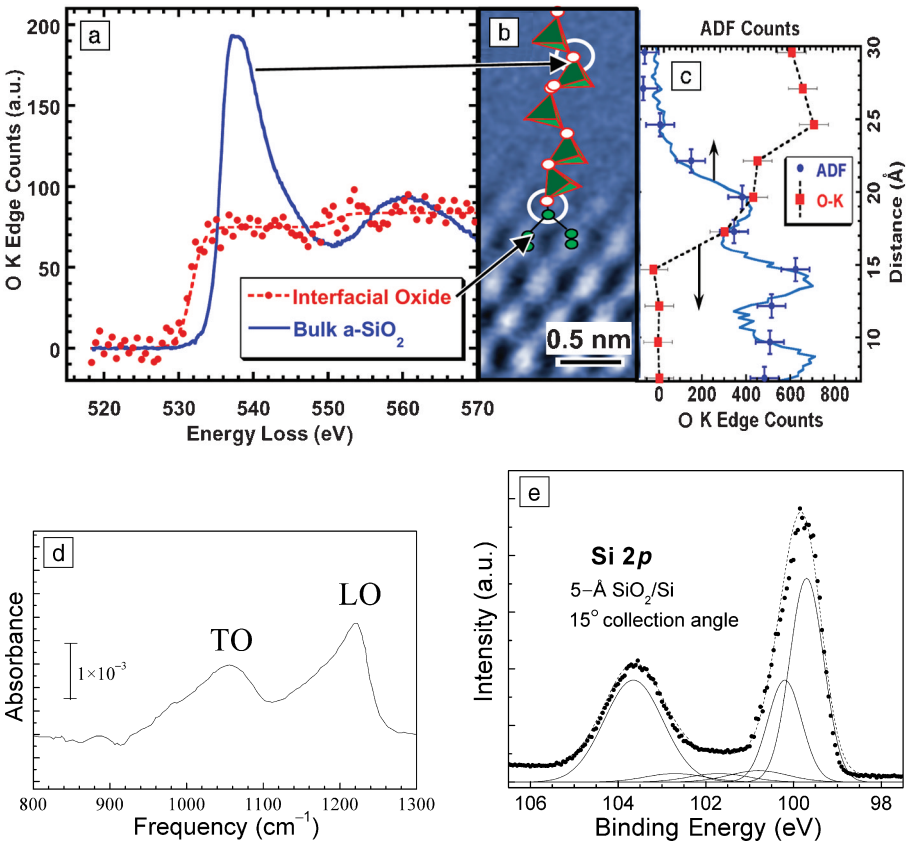

Figure 1. (a) Electron energy-loss spectroscopy (EELS) measurements for oxygen K-edges of bulk amorphous-SiO_2 (a-SiO_2) and for O atoms at an atomically smooth interface between Si(100) and native a-SiO_2. The 3-eV reduction in the edge onset at the interface aligns the unoccupied O interfacial states with the Si conduction band edge, as would be expected for induced gap states. (b) Annular dark-field scanning transmission electron microscopy (ADF-STEM) image of the interface between the a-SiO_2 and the Si substrate, which is used to position the beam for EELS measurements. (c) Measured EELS O K-edge profile (red squares) across the Si/a-SiO_2 interface, and the accompanying ADF signal (blue dots), which is sensitive to the Si profile. The suboxide is the region where the Si and O profiles are half of their bulk intensities (i.e., $Si_{0.5}O_{0.5}$). The layer is broadened by the spatial resolution of the instrument, which after deconvolution is estimated to be less than 2 Å. (d) Infrared-absorption spectrum for a 5-Å SiO_2 film thermally grown on Si, acquired with the infrared beam at off-normal incidence (68°). TO indicates a transverse optical mode; LO indicates a longitudinal optical mode. (e) Si 2p photoelectron spectrum, collected at a 15° take-off angle, for a 5-Å SiO_2 film thermally grown on Si. The data are shown as points. The overall fit, background plus peaks, is shown as lines with the following contributions: Si^{+4}, Si^{+3}, Si^{+2}, Si^{+1}, Si^0 $2p_{1/2}$, and Si^0 $2p_{3/2}$.

the substrate to form new SiO_2) breaks down.[9] It has also been valuable in precision metrology studies of film thickness.[11]

Infrared-absorption spectroscopy (IRAS) is a powerful technique for uncovering the chemical nature of the oxide.[12] Photons are absorbed by exciting vibrations in the material that are characteristic of specific bonding types. Thus, in principle the spectrum reflects the local bonding information. Figure 1d shows, however, that the spectral features associated with a thin (5 Å) SiO_2 film are broad and featureless.[13] For this amorphous matrix, Coulomb and mechanical interactions lead to mode-mixing, preventing precise understanding of local structures. Yet, using grazing incidence diffraction, both the transverse optical (TO) and longitudinal optical (LO) modes are detected, and much can be learned from the dependence of these modes on film thickness. Both undergo a redshift as the oxide is thinned, the magnitude of which is consistent with the existence of a substoichiometric SiO_x oxide within 5 Å of the Si substrate. Within this region, there is, on average, 60% of the oxide with a SiO stoichiometry, encompassing all states of oxidation.[13] The knowledge that the TO and LO bands are located in the range of 1000–1060 cm^{-1} and 1170–1250 cm^{-1}, respectively, even at the interface, makes it possible to determine the amount of SiO_x at the interfaces between Si and high-κ dielectric films, as will be discussed. Finally, we note that IRAS offers one of the only ways to accurately measure H in a film, as most other methods are insensitive to it.

In addition to offering a reasonably accurate determination of the elemental concentration of surface species, x-ray photoelectron spectroscopy (XPS) is probably the most precise method we have to determine the oxidation state of elements at or near a surface. As the XPS peak position is determined by the oxidation state and local electronic environment surrounding each species, the information, while complex, can be quite valuable. For example, spectra in the Si 2*p* energy region are determined by an appropriately weighted convolution of corresponding oxidation states, Si^{+4}, Si^{+3}, Si^{+2}, Si^{+1}, and Si^0 (in addition, each oxidation state presents itself as a spin-orbit split pair, $2p_{1/2}$ and $2p_{3/2}$).[14] Figure 1e shows the XPS Si 2*p* core-level spectrum for a 5-Å thermally grown SiO_2 film, collected at a 15° electron-takeoff angle. Furthermore, by collecting XPS data as a function of the takeoff angle (i.e., angle-resolved XPS, or AR-XPS), one can obtain depth profiles of the various detected species.[15]

Zirconium Oxide

ZrO_2 (as well as HfO_2) has several properties that result in its being a leading candidate for an alternative gate dielectric. The reported dielectric constant is relatively high among the binary-metal oxides ($\kappa \sim 25$). The thermal stability next to Si is very good. Reports have indicated that pure ZrO_2 next to Si (with an ultrathin intervening SiO_x layer) remains stable up to 900°C.[16] Band offsets and barrier heights are suitable. Unfortunately, several problems exist with ZrO_2. Although one prefers an amorphous phase, ZrO_2 films become polycrystalline either during growth or after only moderate postdeposition anneals. This poses a problem for maintaining film and "local" dielectric uniformity over the length scale of future scaled complementary metal oxide semiconductor (CMOS) devices (<0.1 μm), and for maintaining low leakage current, where grain boundaries are proposed to provide easy leakage pathways. This has recently been verified for ZrO_2 films ~50 Å thick deposited by e-beam evaporation in ultrahigh vacuum.[17] In addition, other studies[18–21] have clearly revealed that ultrathin ZrO_2 films are readily traversed by oxygen, leading to

detrimental interfacial growth of a low-κ SiO_2 or silicate layer (see discussion of Figure 2b). Furthermore, it has been reported that atomic layer deposition (ALD) growth of ZrO_2 using $ZrCl_4$ and H_2O as precursors[16] results in poor nucleation unless the growth begins on an SiO_2 or Si-OH terminated layer, thus setting a lower limit to the ultimate achievable electrical thickness.

Physical characterization of ZrO_2 layers by STEM/EELS and MEIS have revealed information about the composition of the ZrO_2/Si interface, as well as oxygen transport and exchange characteristics. Figure 2a shows an ADF-STEM image of a ZrO_2 film grown by chemical vapor deposition (CVD) on a SiO_2 layer. A capping layer of poly-Si was grown above the ZrO_2 layer, and the entire gate stack was annealed at 800°C. The EELS profile across the ZrO_2/poly-Si interface shows that a 7-Å-thick SiO_2 layer has formed between the ZrO_2 and the poly-Si during the annealing process. It is possible that excess O trapped in the ZrO_2 layer has reacted with the silicon in the gate contact. Reactions between the high-κ layer and the gate electrode are not uncommon and are not always confined to the thin reaction zone. For instance, Al electrodes are easily oxidized to form an aluminum oxide layer—often 20 Å or more thick—under typical annealing conditions.[22]

MEIS was used to analyze the O transport and exchange behavior of ZrO_2 films deposited onto H-terminated Si by reactive sputtering.[21] Oxygen transport leading to interfacial SiO_2 growth and a dramatic oxygen exchange were observed for such ZrO_2 films annealed *ex situ* in O_2 after deposition. Figure 2b shows ion-scattering energy spectra for a 45-Å ZrO_2 film as-deposited and after an anneal in 1 Torr $^{18}O_2$ at 800°C for 5 min. The depth profile of the as-deposited film (not shown) reveals a thin (~5 Å) SiO_x layer, formed during the initial deposition of the film (or from subsequent exposure to the atmosphere). Subsequent annealing in isotopically pure $^{18}O_2$ leads to clear SiO_2 growth, as can be seen in the data. The O and Si yields in the energy spectrum are broadened to lower energy, and hence deeper in the film, implying more SiO_x growth at the interface. The Zr yield on the other hand, is only slightly affected, indicating no major change in the Zr depth distribution. The inset of Figure 2b shows the dependence of the interfacial SiO_2 growth on the annealing temperature. A dramatic O exchange also occurs in the film during annealing. This is seen in the data by the increase in the signal of the more massive ^{18}O and corresponding decrease of ^{16}O. Transport of reactive O ions is what likely leads to this rapid interfacial growth through 45 Å of ZrO_2 and the exchange of O within the film. However, grain boundaries and the polymorphic composition of the film are likely to affect the degree of exchange as well.[21]

Many of the weaknesses of the pure ZrO_2 films (namely, low crystallization temperature and rapid oxygen conduction) can be ameliorated by using zirconium silicate or aluminate films instead.[23] Some evidence implies that a relatively high dielectric constant ($\kappa \sim 10$–12) can be preserved even at low Zr concentrations,[23,24] which is fortunate, as only the low-Zr-concentration silicates remain mixed and amorphous upon annealing.[24] Nevertheless, as shown in Figure 3, a 3.5-Å Zr-free region is detected at both interfaces for a $(ZrO_2)_x(SiO_2)_{1-x}$ ($x = 0.15$) composition gate dielectric grown by sputtering.[22,23] In the silicates, this region does not grow under vacuum annealing. Not too surprisingly, the EELS fine structure of the interfacial region resembles that of the interface states in pure SiO_2,[6,22] explaining perhaps the reasonable electrical properties of the "silicate" interfaces. Of more general interest is that the EELS signature of the first 3–5 Å of a Si/SiO_2 interface suggests that this region is likely to possess a higher dielectric constant than bulk SiO_2; thus, provided that the thickness of the Zr-free region is kept to less than 5 Å, it is not expected to severely impact the gate capacitance.[22]

Aluminum Oxide

ALD is a useful technique for growing high-κ dielectrics, particularly when conformality with a patterned substrate is important (see the cover of this issue). In principle, ALD produces layer-by-layer growth, with full monolayer completion at each step including the first dielectric layer. In practice, the growth of the initial layer is not straightforward, as illustrated in the case for Al_2O_3.

Aluminum oxide is grown on either H-passivated or oxidized silicon surfaces by sequential pulsed exposures to H_2O and

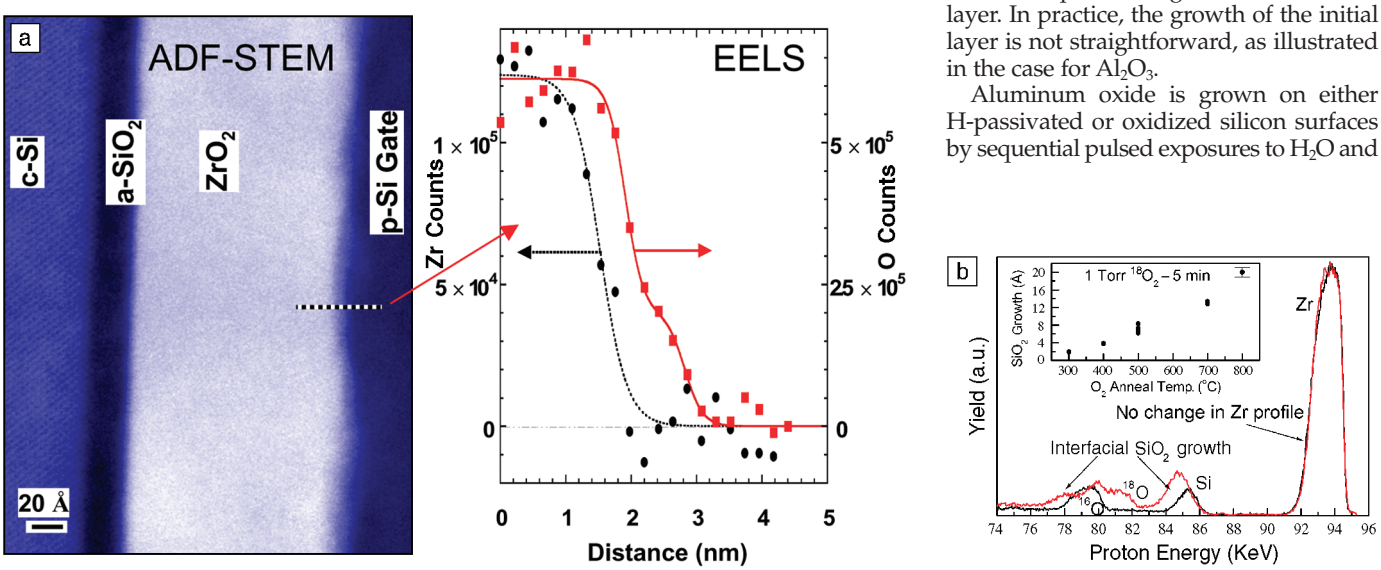

Figure 2. (a) ADF-STEM image of a ZrO_2 film grown on SiO_2, then capped with poly-Si and annealed at 800°C. The EELS profile across the ZrO_2/poly-Si interface shows the O signal extends 7 Å beyond the Zr signal into the poly-Si region, indicative of a thin SiO_2 layer. This is confirmed by the EELS fine structure (not shown), which bears the fingerprint of SiO_2 bonding. (b) Ion-scattering energy spectra of a 45-Å ZrO_2 film as-deposited and after a 1 Torr/5 min/800°C anneal in $^{18}O_2$. Interfacial SiO_2 growth and O exchange are easily seen. The inset shows the amount of SiO_2 growth versus the annealing temperature.

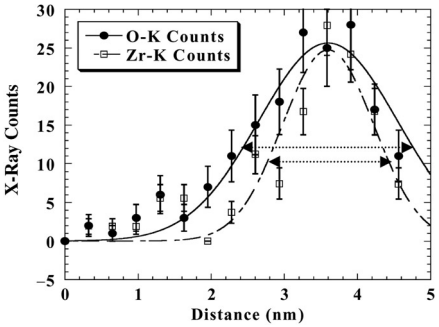

Figure 3. EELS O and Zr profiles from a $Si/(ZrO_2)_{0.15}(SiO_2)_{0.85}/Si$ gate stack after annealing. The full width at half maximum (FWHM) of the O EELS edge profile is 21 ± 1 Å. The FWHM of the Zr profile is 14 ± 1 Å. The narrower Zr distribution implies that there is 3.5 ± 0.5 Å of Zr-free oxide at each of the Si/dielectric interfaces.

trimethylaluminum (TMA),[25–27] producing OH and Al-$(CH_3)_n$ terminated surfaces, respectively. For growth on H-terminated silicon surfaces, there is an incubation period, in contrast to growth on oxidized silicon, after which the film grows linearly with the number of water/TMA pulses. This observation indicates that a single H_2O pulse (or even several pulses) is not sufficient to hydroxylate the surface. In addition, there is evidence (see subsequent discussion) that a thin SiO_x layer is produced in the process which appears to be necessary for subsequent Al_2O_3 growth. Such a layer lowers the effective dielectric constant of the film and is therefore detrimental to the device performance sought.

Central to this initial step is an understanding of oxygen incorporation into H-passivated surfaces. Early IRAS studies of O_2 oxidation of H/Si(111) suggest that oxygen can be incorporated at 575 K, without removal of the surface hydrogen.[28–30] More recently, O_2 oxidation of HF-etched Si(100) was found to proceed with an activation energy of 1.6 eV and 1.7 eV for di- and monohydride, respectively, again without removal of the surface hydrogen.[31] Preliminary studies of H_2O interaction with H-passivated silicon surfaces suggest that oxygen is inserted with similar activation energies and without surface H removal.[32] If this is the case, it is unlikely that a uniform hydroxyl layer is formed. Instead, oxidation takes place prior to H removal, leading to a nonideal interface.

The interfacial region can be studied with a combination of AR-XPS, IRAS, and ADF-STEM. Converting AR-XPS data to an elemental depth profile, Al_2O_3 films grown on Si with and without an initial SiO_2 layer are analyzed as shown in Figures 4a and 4b, which show depth profiles for Si, Al, O, and C. The film grown on the SiO_2 layer is substantially thicker than the film grown on H-terminated Si because growth can start right away on the oxide (no incubation period). Since the Si^{+4} signal is so weak, the maximum entropy algorithm has difficulty placing the oxide layer at the Al_2O_3/Si interface. Based on comparisons with 5-Å SiO_2 films,[13] XPS indicates that the interfacial SiO_2 layer for growth on HF-etched Si is less than 2 Å thick. IRAS data corresponding to the films in Figures 4a and 4b are shown in Figures 4c and 4d, respectively. The Al_2O_3 TO modes are broad and featureless (best seen in the *s*-polarization data in the range of 500–800 cm^{-1}), while the Al_2O_3 LO modes display a well-defined peak at 957 cm^{-1}. For films grown on a thin oxide, the SiO_2 TO and LO modes are clearly seen at 1035 cm^{-1} and 1230 cm^{-1}, respectively. Using this information, and the fact that any Si-O vibration for sub-stoichiometric silicon oxide falls in the 1000–1200 cm^{-1} range, we estimate that the SiO_x layer present on silicon with no intentional oxide is 1.5 ± 0.5 Å.

Such an extremely thin SiO_x layer is not detectable with conventional TEM (Figure 5a), as the low-angle electron-scattering amplitudes for Al and Si are very similar.[33] However, ADF-STEM measures the high-angle scattering, which is roughly proportional to the square of the atomic number (hence it is sometimes called Z-contrast STEM),[34] and is sufficiently sensitive to resolve the interlayer (Figure 5b).

Another important issue facing the atomic layer growth of Al_2O_3 is the presence of hydroxide in the film. The breadth and the position of the O 1*s* peak suggest that there is more than one binding state for O in the films. Although this other binding state cannot be unambiguously resolved, the likely binding energy of these photoelectrons is consistent with hydroxide mixed with oxide. The O/Al ratio is also found to be significantly greater than the 1.5 expected for pure Al_2O_3. Angle-resolved photoemission suggests that this hydroxide species is present in the outer third of the film, and annealing at 400°C *in vacuo* reduces the O content of the film and narrows the O 1*s* photoelectron peak width, but does not show evidence for reduced Al. Returning the specimen to ambient laboratory conditions for 24 h shows that the hydroxide component reappears. This result is consistent with the MEIS results that suggest that the Al_2O_3 films are not fully dense as-deposited.

MEIS analysis of thin Al_2O_3 films on Si is made difficult by the similar masses of Al and Si, so resolving very thin (~1–2 Å)

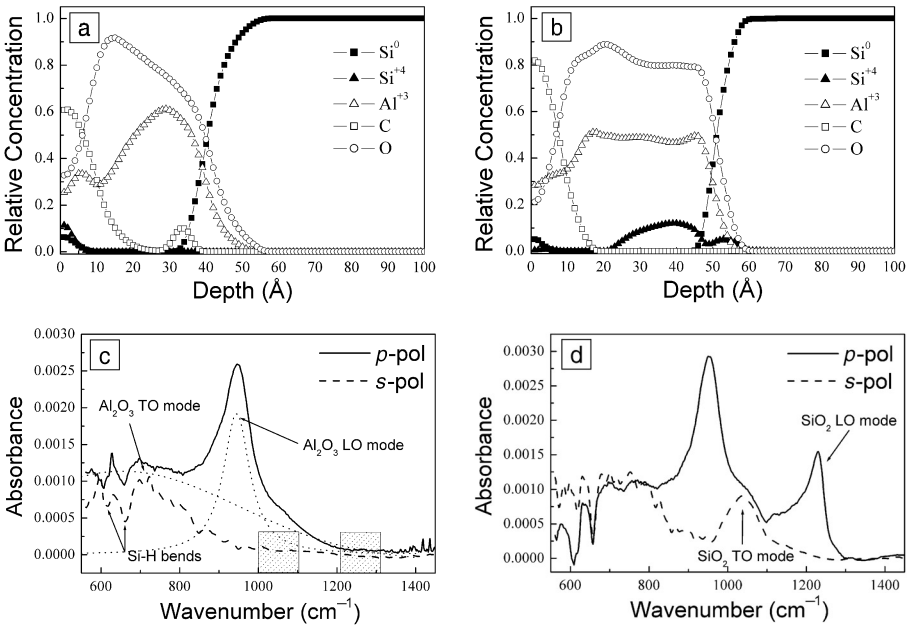

Figure 4. Depth profiles of Al_2O_3 films grown by atomic layer deposition (ALD) under identical conditions (a) on H-terminated Si and (b) with an approximately 5-Å layer of SiO_2. The depth profiles were determined by applying the maximum entropy algorithm to angle-resolved photoemission. Infrared-absorption spectra of the same two samples are shown in (c) and (d). The hatched areas correspond to where the interfacial SiO_x modes are expected.

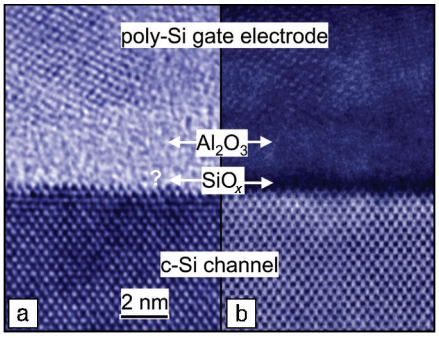

Figure 5. (a) Conventional TEM image of an ALD-grown Al_2O_3 gate oxide. This image is more sensitive to crystalline order than chemical composition, so the SiO_2 interlayer is not observed. (b) ADF (or Z-contrast) STEM image showing the thin (<0.3 nm) SiO_2 layer that forms during the initial stages of ALD growth on the silicon substrate.

interfacial SiO_2 is difficult. One way around this problem is to use nuclear resonant profiling.[11,33] Using the $^{27}Al(p,\gamma)^{28}Si$ resonance renders an Al depth profile in a Si matrix with a depth resolution comparable to MEIS. Under certain conditions, however, MEIS can still provide accurate information on Al_2O_3 films. For instance, a combined TEM/MEIS experiment has revealed that the density of ALD Al_2O_3 films (even after an 800°C anneal) is substantially less than the bulk Al_2O_3 value (2.94 g/cm^3, compared with 3.97 g/cm^3). MEIS was used to determine the number of Al and O atoms in an Al_2O_3 film grown on top of a thick (30 Å) SiO_2 layer. Knowledge of the MEIS energy spectrum of the thick SiO_2 film prior to ALD growth allowed for an accurate deconvolution of the Al signal. This result, combined with the accurate thickness given by TEM, yielded the density.

Yttrium and Gadolinium Oxides

As with the oxides discussed previously in this article, the rare-earth oxides are attractive candidates for alternative gate dielectrics based on thermodynamics considerations and their moderately high dielectric constants. For example, Y_2O_3 and Gd_2O_3 possess intermediate dielectric constants of ~18 and ~14, respectively. A serious problem, however, is that rare-earth oxides are known to be hygroscopic. That is, with increasing ionicity in binary oxides, reactions with water become a greater problem, leading to hydroxide formation after exposure of a thin film to atmospheric conditions. Using e-beam evaporation in ultrahigh vacuum,[35,36] followed by *in situ* capping with a-Si, Y_2O_3 and Gd_2O_3 layers show no SiO_xH_y underlayer. On the other hand, uncapped films that are exposed to atmosphere (or are capped, but are thinned too much for TEM preparation) show SiO_xH_y at the substrate interface as well as an excess of O in the bulk of the film (due to hydroxide formation). TEM/EELS[36] and MEIS[37] have clearly revealed these effects.

The reactivity of rare-earth oxides with water is a serious problem for TEM measurements, as samples must be made very thin. However, the reaction layer is about 30 Å thick (on each side of the cross-sectional sample). The challenge is then to keep samples thick enough that this reaction layer is a small fraction of the film thickness. In such thick samples, there is often too much elastic scattering for meaningful EELS measurements, while atomic-resolution ADF imaging is still practical. Figure 6a shows the absence of an interfacial layer for a thick cross section of a capped Y_2O_3 layer, while Figure 6b reveals detection of a hydroxide layer in a thin cross-sectioned region of the same sample. The hydroxide phases for La_2O_3, Y_2O_3, ZrO_2, and Gd_2O_3 can be readily detected by EELS, as they generally result in a rounded O K-edge instead of the characteristic double-peak splitting expected for O bonded to transition metals. An example of an O K-edge from a hydroxide layer can be found in the literature.[38]

Oxygen uptake and reaction with the oxide/substrate interface is also revealed by MEIS depth profiling.[37] Figure 6c shows MEIS depth profiles for a thin Y_2O_3 layer that was capped in ultrahigh vacuum prior to exposure to the air. The film is stoichiometric (Y_2O_3), and exhibits a sharp (≤2 Å) interface to the substrate. IRAS measurements also support this conclusion.[36] Reaction of an uncapped Y_2O_3 layer with O-containing molecules in air leads to an excess of O in the film ($Y_2O_{x>3}$) and to an interfacial layer (6–8 Å) of primarily SiO_x (Figure 6d).

MEIS depth-profiling analysis also revealed differences in the reactivity of the Y_2O_3 layer with the substrate, depending on whether the layer was capped or not. Si uptake from the substrate occurred at 700°C for uncapped films, likely due to the reaction of Si with the excess O in the layer to form a silicate. On the other hand, the sharp interfaces present for capped films remained sharp for vacuum anneals of up to 900°C.

Summary and Outlook

In this article, we have summarized the strengths and capabilities of several techniques used for the physical characterization of alternative gate dielectrics. It is only through the use of several complementary techniques such as these that a full understanding of a given physical system can be reached. Composition information is given by all four techniques, while depth profiling is available in STEM/EELS, XPS, and MEIS. Chemical information is given by EELS, IRAS, and XPS. Finally, structural information is provided by STEM, IRAS, and MEIS. The complementary nature of and overlap of abilities in these techniques

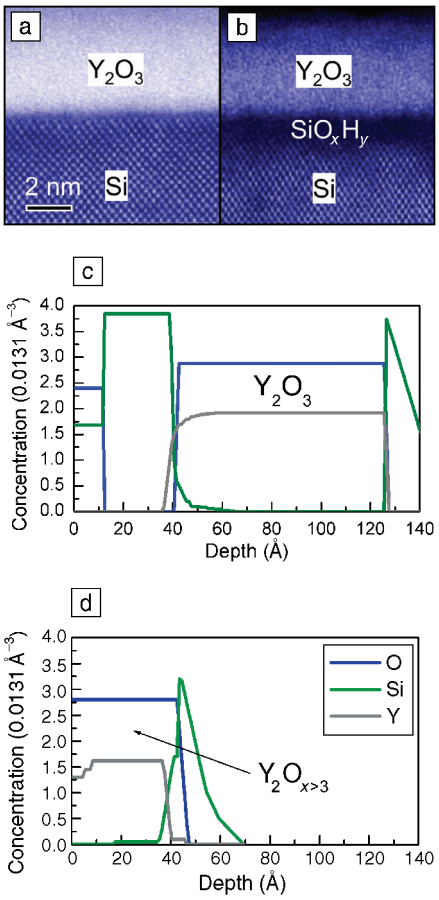

Figure 6. (a) ADF-STEM image of a capped Y_2O_3/Si sample, which is thick enough that surface reaction layers are not visible. (b) The same Y_2O_3/Si sample in a thinner region. Not only has a hydroxide formed on the entrance and exit surfaces, but the capping layer has also been milled away, and the hydroxide reaction layers dominate the interface contrast. MEIS depth profiles of in situ *(c) Si-capped and (d) uncapped Y_2O_3 layers. Capped films are stoichiometric Y_2O_3 and exhibit a sharp interface to the substrate. Uncapped films contain an excess of O throughout the film, as well as a SiO_x interfacial layer.*

are critical. Several aspects concerning the makeup and interfaces of alternative gate dielectrics are beginning to be understood. For instance, it has become clear from STEM/EELS and MEIS that ZrO_2 is very transparent to oxygen, and that small partial pressures of O will lead to undesired interfacial SiO_2 formation during thermal processing. Rare-earth oxides, such as Y_2O_3 and Gd_2O_3, are extremely susceptible to hydroxide formation when exposed to the ambient atmosphere. MEIS and XPS clearly show the presence of excess O, while XPS provides the chemical information suggesting how this excess O is bonded in the film. Capping of rare-earth oxides prior to atmospheric exposure is necessary, and using the extreme sensitivity of IRAS, SiO_2-free interfaces have been made. The interfacial and chemical makeup of ALD-grown Al_2O_3 has been of significant interest lately. In particular, it is becoming clear that the initial hydroxilization with water of the HF-etched Si surface does not proceed by simply terminating the Si surface with OH groups, but rather involves incorporation of sub-surface oxygen without removal of the surface hydrogen. ADF-STEM and IRAS support the formation of a very thin SiO_x layer at the interface. Complementary chemical techniques such as IRAS and XPS are helping to shed light on the physical mechanisms of the initial ALD growth, and perhaps might indicate ways in which the growth can be better started. One interesting area of future work involves using IRAS to investigate the role that hydrogen plays in high-κ films.

Acknowledgment

The authors would like to acknowledge their extensive interactions with Marty Green, Torgny Gustafsson, Hartmut Schulte, and Glen Wilk on various parts of this work. B. Busch and E. Garfunkel also acknowledge the support of the Semiconductor Research Center, Agere Systems, and Lucent Technologies.

References

1. N.D. Browning, M.M. Chisholm, and S.J. Pennycook, *Nature* **366** (1993) p. 143.
2. D.A. Muller, Y. Tzou, R. Raj, and J. Silcox, *Nature* **366** (1993) p. 725.
3. P.E. Batson, *Nature* **366** (1993) p. 728.
4. J.B. Neaton, D.A. Muller, and N.W. Ashcroft, *Phys. Rev. Lett.* **85** (2000) p. 1298.
5. R.F. Egerton, *Electron Energy Loss Spectroscopy in the Electron Microscope* (Plenum Publishers, New York, 1996).
6. D.A. Muller, T. Sorsch, S. Moccio, F.H. Baumann, K. Evans-Lutterodt, and G. Timp, *Nature* **399** (1999) p. 758.
7. D.A. Muller, in *Proc. 2000 Int. Conf. on Characterization and Metrology for ULSI Technology* (American Institute of Physics, College Park, MD, 2000) p. 500.
8. J.F. van der Veen, *Surf. Sci. Rep.* **5** (1985) p. 199.
9. E.P. Gusev, H.C. Lu, T. Gustafsson, and E. Garfunkel, *Phys. Rev. B* **52** (1995) p. 1759.
10. H.C. Lu, E.P. Gusev, E. Garfunkel, B.W. Busch, T. Gustafsson, T.W. Sorsch, and M.L. Green, *J. Appl. Phys.* **87** (2000) p. 1550.
11. W.H. Schulte, B. Busch, E. Garfunkel, and T. Gustafsson, in *Handbook of Silicon Semiconductor Metrology*, edited by A.C. Diebold (Marcel Dekker, New York, 2001) p. 811.
12. Y.J. Chabal, M.K. Weldon, and K.T. Queeney, in *Fundamental Aspects of Silicon Oxidation*, Springer Series in Materials Science, Vol. 46, edited by Y.J. Chabal (Springer, Berlin, 2001) p. 143.
13. K.T. Queeney, M.K. Weldon, J.P. Chang, Y.J. Chabal, A.B. Gurevich, J. Sapjeta, and R.L. Opila, *J. Appl. Phys.* **87** (2000) p. 1322.
14. F.J. Himpsel, F.R. McFeely, A. Taleb-Ibrahimi, J.A. Yarmoff, and G. Hollinger, *Phys. Rev. B* **38** (1988) p. 6084.
15. J.P. Chang, M.L. Green, V.M. Donnelly, R.L. Opila Jr., J. Eng, J. Sapjeta, P.J. Silverman, B. Weir, H.C. Lu, T. Gustafsson, and E. Garfunkel, *J. Appl. Phys.* **87** (2000) p. 4449.
16. M. Copel, M. Gribelyuk, and E.P. Gusev, *Appl. Phys. Lett.* **76** (2000) p. 436.
17. J. Kwo (unpublished).
18. T.S. Jeon, J.M. White, and D.L. Kwong, *Appl. Phys. Lett.* **78** (2001) p. 368.
19. Y.-M. Sun, J. Lozano, H. Ho, H.J. Park, S. Veldman, and J.M. White, *Appl. Surf. Sci.* **161** (2000) p. 115.
20. B.H. Lee, L. Kang, R. Nieh, W.J. Qi, and J.C. Lee, *Appl. Phys. Lett.* **76** (2000) p. 1926.
21. B.W. Busch, W.H. Schulte, E. Garfunkel, T. Gustafsson, W. Qi, R. Nieh, and J. Lee, *Phys. Rev. B* **62** (2000) p. R13290.
22. D.A. Muller and G.D. Wilk, *Appl. Phys. Lett.* **79** (2001) p. 4195.
23. G.D. Wilk and R.M. Wallace, *Appl. Phys. Lett.* **76** (2000) p. 112.
24. G. Lucovsky and G.B. Rayner Jr., *Appl. Phys. Lett.* **77** (2000) p. 2912.
25. G.S. Higashi and C.G. Fleming, *Appl. Phys. Lett.* **55** (1989) p. 1963.
26. P. Ericsson, S. Bengtsson, and J. Skarp, *Microelectron. Eng.* **36** (1997) p. 91.
27. M. Juppo, A. Rahtu, M. Ritala, and M. Leskelä, *Langmuir* **16** (2000) p. 4043.
28. T. Hattori, T. Aiba, E. Iijima, Y. Okube, H. Nohira, N. Tate, and M. Katayama, *Surf. Sci.* **104/105** (1996) p. 323.
29. H. Ikeda, Y. Nakagawa, M. Toshima, S. Furuta, S. Zaima, and Y. Yasuda, *Surf. Sci.* **117/118** (1997) p. 109.
30. H. Ikeda, Y. Nakagawa, S. Zaima, Y. Ishibashi, and Y. Yasuda, *Jpn. J. Appl. Phys.* **38** (1999) p. 3422.
31. X. Zhang, Y.J. Chabal, and E. Garfunkel, *J. Vac. Sci. Technol., A* **19** (2001) p. 1725.
32. X. Zhang, Y.J. Chabal, E. Garfunkel, and S.B. Christman, *Appl. Phys. Lett.* **79** (2001) p. 4051.
33. E.P. Gusev, M. Copel, E. Cartier, I.J.R. Baumvol, C. Krug, and M.A. Gribelyuk, *Appl. Phys. Lett.* **76** (2000) p. 176.
34. A. Howie, *J. Microscopy* **17** (1979) p. 11.
35. J. Kwo, M. Hong, A.R. Kortan, K.T. Queeney, Y.J. Chabal, J.P. Mannaerts, T. Boone, J.J. Krajewski, A.M. Sergent, and J.M. Rosamilia, *Appl. Phys. Lett.* **77** (2000) p. 130.
36. J. Kwo, M. Hong, A.R. Kortan, K.T. Queeney, Y.J. Chabal, R.L. Opila, D.A. Muller, S.N.G. Chu, B.J. Sapjeta, T.S. Lay, J.P. Mannaerts, T. Boone, H.W. Krautter, J.J. Krajewski, A.M. Sergent, and J.M. Rosamilia, *J. Appl. Phys.* **89** (2001) p. 3920.
37. B.W. Busch, J. Kwo, M. Hong, J.P. Mannaerts, B.J. Sapjeta, W.H. Schulte, E. Garfunkel, and T. Gustafsson, *Appl. Phys. Lett.* **79** (2001) p. 2447.
38. S. Stemmer, J.-P. Maria, and A.I. Kingon, *Appl. Phys. Lett.* **79** (2001) p. 104. □